J Arid Land (2022) 14(4): 426–440
https://doi.org/10.1007/s40333-022-0013-0

Science Press Springer-Verlag

Application of the InVEST model for assessing water yield and its response to precipitation and land use in the Weihe River Basin, China

WU Changxue[1], QIU Dexun[2,3], GAO Peng[1,2,3*], MU Xingmin[1,2,3*], ZHAO Guangju[1,2,3]

[1] State Key Laboratory of Soil Erosion and Dryland Farming on the Loess Plateau, Institute of Soil and Water Conservation, Northwest A&F University, Yangling 712100, China;
[2] State Key Laboratory of Soil Erosion and Dryland Farming on the Loess Plateau, Institute of Soil and Water Conservation, Chinese Academy of Sciences and Ministry of Water Resources, Yangling 712100, China;
[3] University of Chinese Academy of Sciences, Beijing 100000, China

Abstract: With realizing the importance of ecosystem services to society, the efforts to evaluate the ecosystem services have increased. As the largest tributary of the Yellow River, the Weihe River has been endowed with many ecological service functions. Among which, water yield can be a measure of local availability of water and an index for evaluating the conservation function of the region. This study aimed to explore the temporal and spatial variation of water yield and its influencing factors in the Weihe River Basin (WRB), and provide basis for formulating reasonable water resources utilization schemes. Based on the InVEST (integrated valuation of ecosystem services and tradeoffs) model, this study simulated the water yield in the WRB from 1985 to 2019, and discussed the impacts of climatic factors and land use change on water yield by spatial autocorrelation analysis and scenario analysis methods. The results showed that there was a slight increasing trend in water yield in the WRB over the study period with the increasing rate of 4.84 mm/10a and an average depth of 83.14 mm. The main water-producing areas were concentrated along the mainstream of the Weihe River and in the southern basin. Changes in water yield were comprehensively affected by climate and underlying surface factors. Precipitation was the main factor affecting water yield, which was consistent with water yield in time. And there existed significant spatial agglomeration between water yield and precipitation. Land use had little impact on the amount of water yield, but had an impact on its spatial distribution. Water yield was higher in areas with wide distribution of construction land and grassland. Water yield of different land use types were different. Unused land showed the largest water yield capacity, whereas grassland and farmland contributed most to the total water yield. The increasing water yield in the basin indicates an enhanced water supply service function of the ecosystem. These results are of great significance to the water resources management of the WRB.

Keywords: water yield; InVEST model; Weihe River Basin; Geoda model; scenario analysis

Citation: WU Changxue, QIU Dexun, GAO Peng, MU Xingmin, ZHAO Guangju. 2022. Application of the InVEST model for assessing water yield and its response to precipitation and land use in the Weihe River Basin, China. Journal of Arid Land, 14(4): 426–440. https://doi.org/10.1007/s40333-022-0013-0

1 Introduction

Ecosystems directly or indirectly provide various services to human beings (Symmank et al., 2020), which were defined as "the benefits that humans derive from nature" (Hassan and Scholes,

*Corresponding author: GAO Peng (E-mail: gaopeng@ms.iswc.ac.cn); MU Xingmin (E-mail: xmmu@ms.iswc.ac.cn)
Received 2022-02-06; revised 2022-03-31; accepted 2022-04-18

2005). As the attribute of the ecosystem and the key component of an ecological process, water yield can produce water-related ecosystem services (Costanza et al., 1998). For example, it regulates surface runoff over the dry and flood seasons, reduces potential drought and flood risks, and ensures drinking water sources (Zhang et al., 2010). In summary, water yield is a resource supporting human life and development, such as agriculture, industry, human consumption, hydropower, fisheries, and recreational activities (Natalia et al., 2015).

The growth in the global human population, the improvement in living standards, changes in consumption patterns, and the expansion of irrigated agriculture over the last few decades has resulted in a gradual increase in the demand for water resources (Ercin and Hoekstra, 2014; Gómez et al., 2014; Vorosmarty et al., 2000). Consequently, many countries are facing increasing water scarcity challenges (Qiu, 2010; Liu and Wu, 2012; Mekonnen and Hoekstra, 2016). In China, high demand for food and the imbalance of regional economic development have resulted in increased water resources utilization and uneven distribution (Mekonnen and Hoekstra, 2016). Relevant studies have shown a sharp decrease in measured runoff in major river basins of China in recent decades (Xu et al., 2010). The changes to water resources of the Yellow River have attracted more attention for the importance of this river in China (Qiang et al., 2009). In the late 1990s, the average runoff entering the Yellow River was only 35.99×10^8 m^3, a decrease of 62.06×10^8 m^3, compared with the 1950s (Xia et al., 2007). And this runoff further decreased in the 21st century (Zhao et al., 2018).

The Weihe River is the largest tributary of the Yellow River and provides irrigation water for nearly 1×10^4 km^2 of farmland in Guanzhong Plain, supporting nearly 61% of the population, 56% of cultivated land, and 81% of gross domestic product (GDP) in Shaanxi Province, China (Liu and Hu, 2008). However, the imbalance between water supply and demand in the Weihe River Basin (WRB) have intensified due to impacts of rapid human development, the construction of water conservancy, soil conservation projects, and other engineering measures (Ma et al., 2008; Cheng et al., 2019; Xu et al., 2021). Information in the Shannxi Water Resources Bulletin (2019) states that agriculture is the sector consuming the most water in the basin (55.13×10^8 m^3), which includes forestry, animal husbandry, fishery, and livestock farming, accounting for 60% of total water consumption; The water consumption of industry and municipal use was 14.85×10^8 and 14.28×10^8 m^3, accounting for 16.05% and 14.12% of total water consumption, respectively. Water consumption in the basin will increase further with the development of economy, imposing more pressure on available water resources (Zhang et al., 2016).

The WRB belongs to a typical transition climate zone in the arid and semi-arid area of northwestern China, and water resources in this area are sensitive to climate change (Chen et al., 2013). Global climate variability over the last few centuries has been characterized by temperature rise and precipitation changes. These changes have had a destructive impact on the natural ecosystem, human economic, and social development (Milliman et al., 2008). Water yield has gradually become an important factor restricting the sustainable development of society. Therefore, an evaluation of water yield of the WRB is of great significance.

Model can be a useful tool for the evaluation of water-related ecosystem service functions and the quantitative estimation of water yield under various conditions. The models include soil and water assessment tool (SWAT) (Baker and Miller, 2013; Gassman et al., 2017), social values for ecosystem services (SolVES) (Greg et al., 2012; Sherrouse et al., 2011), multi-scale integrated models of ecosystem services (MIMES) (Boumans and Costanza, 2008), and integrated valuation of ecosystem services and tradeoffs (InVEST) (Sharp et al., 2020). Among these models, the InVEST model has been the most widely applied due to its less data requirement and ability to visualize simulation results (Huang et al., 2013; Scordo et al., 2018; Cara et al., 2020). The InVEST model integrates a series of ecosystem processes, and can simulate the quality and value of ecosystem services regulated by land use, physical environmental factors, and socio-economic factors (Jiang et al., 2021). Numerous studies have applied it to various regions of the world and

have achieved good results, such as North Korea (Kim and Jung, 2020), the Wildcat Creek Watershed in Indiana, the Upper Upatoi Creek Watershed in Georgia, the United States (Dennedy-Frank et al., 2016), and some regions of China (Yang et al., 2019; Yin et al., 2020; Li et al., 2021). However, there have been few attempts to apply the InVEST model to the WRB. Those few studies that have applied the InVEST model to the WRB were not able to identify the temporal and spatial variation characteristics in water yield due to their short study periods. Most of these studies also only analyzed the quantitative relationships between water yield and driving factors (Yang et al., 2019), while not analyzing their spatial correlations.

The present study used the InVEST model to (1) simulate water yield of the WRB from 1980 to 2019, and analyze its spatiotemporal variation; (2) identify the main factors regulating water yield under different climate factors and land use types; and (3) discuss the mechanism of regulating water yield.

2 Materials and methods

2.1 Study area

The Weihe River originates from Niaoshu Mountain, Weiyuan County, Gansu Province, following which it flows through the Ningxia Hui Autonomous Region and Shaanxi Province from east to west, including 10 regions and 84 counties. The Weihe River merges into the Yellow River eventually at Tongguan County, Shaanxi Province, China. As the largest tributary of the Yellow River, the Weihe River has a total length of 818 km, and drains an area of 13.5×10^4 km^2. WRB located in the southeastern Loess Plateau, China (33°42′−37°20′N, 106°18′−110°37′E). The terrain of the WRB gradually decreases from west to east. And there is an elevation difference of over 3000 m a.s.l. (Fig. 1). The climate of the WRB is cold and dry in winter, and hot and rainy in summer. The annual average temperature and average annual precipitation are 7.8℃−13.5℃ and 572 mm, respectively.

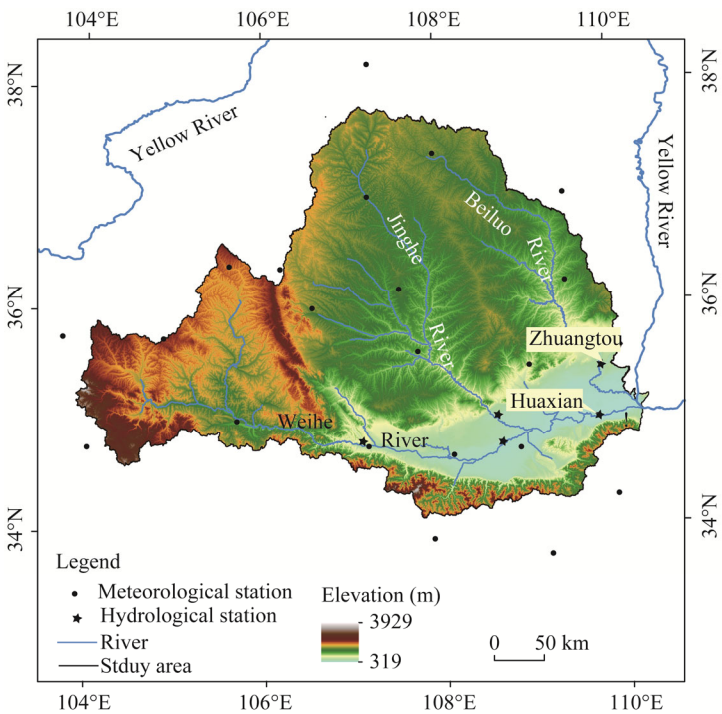

Fig. 1 Elevation, and hydrological and meteorological stations in the Weihe River Basin, China

2.2 Data sources

The data required by the model include meteorological, soil and land use/land cover (LULC) data. The raster input data for the model were derived directly or indirectly from these data. Table 1 summarizes the relevant basic data used in the present study.

Table 1 Relevant basic data sources and description

Data	Data description	Data source
Climate data	Daily precipitation Daily maximum temperature Daily minimum temperature Daily mean temperature	China Meteorological Science Data Sharing Service Network (http://www.cma.gov.cn/)
Soil data	Soil texture (clay, sand, and silt) Soil organic carbon Soil depth	Harmonized World Soil Database (HWSD)
Land use/land cover	Land use/land cover during 1980–2020 at 1 km spatial resolution	Resource and Environmental Science Data Center, Chinese Academy of Sciences (http://www.resdc.cn)
Digital elevation model (DEM)	Elevation of the Weihe River Basin at 30 m spatial resolution	Geospatial Data Cloud Platform of Chinese Academy of Sciences (https://www.gscloud.cn/)
Streamflow data	Measured runoff of Huaxian and Zhuangtou hydrological stations from 1980 to 2019	Yellow River Hydrological Yearbook
Runoff data	Restored runoff of Huaxian and Zhuangtou hydrological stations from 1980 to 1984	Runoff data of the Yellow River Basin

2.3 InVEST model

2.3.1 Introduction of the InVEST model

Budyko curve (Budyko, 1974), and annual average precipitation (P) were used in the InVEST model to calculate water yield. Water yield simulated by the model represents the water outflow from the landscape, including surface flow, underground flow, and base flow (Sharp et al., 2020). The model assumes that water yield of a pixel reaches the specified outlet through one of several paths mentioned above (Zhang et al., 2004; Donohue et al., 2012). The formula is expressed as:

$$Y(x)=\left(1-\frac{\mathrm{AET}(x)}{P(x)}\right)\times P(x), \tag{1}$$

where AET(x) is the annual actual evapotranspiration (mm); and $P(x)$ is the precipitation for a pixel (mm).

For vegetation-covered land, $\frac{\mathrm{AET}(x)}{P(x)}$ was calculated (Fu, 1981; Zhang et al., 2004):

$$\frac{\mathrm{AET}(x)}{P(x)}=1+\frac{\mathrm{PET}(x)}{P(x)}-\left[1+\left(\frac{\mathrm{PET}(x)}{P(x)}\right)^{\omega}\right]^{1/\omega}, \tag{2}$$

where PET(x) is the potential evapotranspiration (mm); and $\omega(x)$ is a nonphysical parameter characterizing regional climate and soil conditions, ranging from 1.25 to 5.00 (Yang et al., 2008; Donohue et al., 2012). The minimum value can be selected when the root depth is 0 cm (bare soil), and is calculated as:

$$\omega(x)=Z\frac{\mathrm{AWC}(x)}{P(x)}+1.25, \tag{3}$$

where Z is the local P and other hydrogeological features, with possible values of 1 to 30; and AWC(x) is the plant available water capacity (mm), and is calculated as:

$$\mathrm{AWC}(x)=\min(\text{rest layer depth},\text{root depth})\times \mathrm{PAWC}, \tag{4}$$

where PAWC is the plant available water capacity (Fig. 2a); and rest layer depth is the depth of

root restricted layer, often expressed as the depth at which 95% of root biomass of the plant (Fig. 2b).

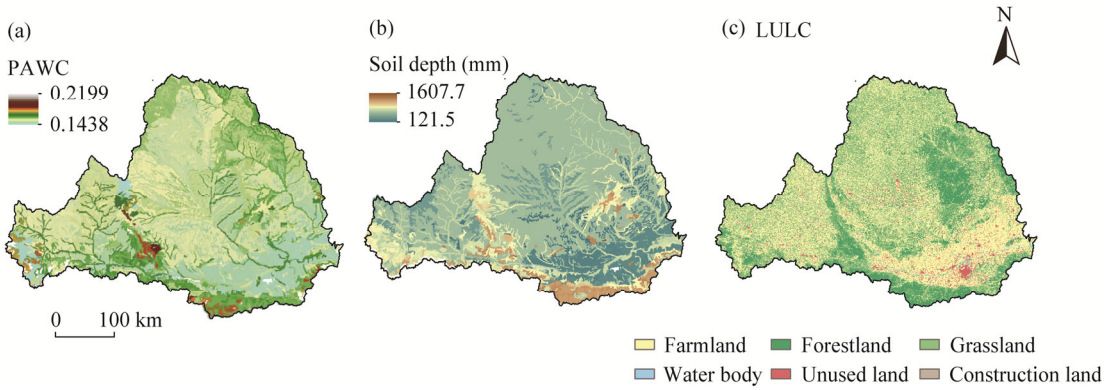

Fig. 2 Spatial distributions of biophysical characteristics of the Weihe River Basin, China. (a), PAWC, plant available water capacity; (b), soil depth; (c), land use/land cover (LULC) in 2020.

2.3.2 Data preparation

The data input to the model included rasterized annual P, average annual ET_0, LULC, depth of the root restricting layer, PAWC, the layers of watersheds and sub-watersheds, the biophysical table, and an appropriate Z parameter (Sharp et al., 2020). All raster data used in the present study were unified into the Krasovsky_1940_Albers coordinate system before input. The sections below describe the processing methods used.

(1) P and ET_0

The annual P and ET_0 data were obtained by adding the daily precipitation and monthly ET_0 data within a year, and Kriging was then used to interpolate the data of 22 meteorological stations around the WRB, which provided a value for each cell in the raster. ET_0 was calculated by the modified Hargreaves equation (Droogers and Allen, 2002):

$$ET_0 = 0.0013 \times 0.408 \times RA \times (T_{av} + 17) \times (TD - 0.0123P)^{0.76}, \quad (5)$$

where T_{av} is the average of mean T_{max} and T_{min} for every month (℃), respectively; TD is the difference between mean T_{max} and T_{min} for every month (℃); and RA is the extraterrestrial radiation (MJ/(m^2·d)). Radiation data were obtained from the United Nations Food and Agriculture Organization (FAO) Irrigation Drainage Paper (Fao et al., 1982).

(2) PAWC

PAWC (Fig. 2a) is the field capacity minus wilting point, ranging from 0 to 1, which was calculated as (Zhou et al.; 2005):

$$PAWC = 54.509 - 0.132 \times sand - 0.003 \times (sand)^2 - 0.055 \times silt - 0.006 \times (silt)^2 - 0.738 \times clay + 0.007 \times (clay)^2 - 2.688 \times OM + 0.501 \times (OM)^2, \quad (6)$$

where sand, silt, clay, and organic matter (OM) were expressed as percentages (%).

(3) LULC

ArcGIS 10.2 was used to reclassify 25 secondary land use types into 6 primary land types (Fig. 2c): farmland, forestland, grassland, water body, construction land, and unused land.

(4) Watershed and sub-watershed

In Arcgis10.2, through the hydrology tool, the WRB was finally divided into 377 sub-watersheds by setting the threshold flow accumulation (TFA) to 4×10^5 m^3.

(5) Biophysical table

The biophysical table (Table 2) contains the information for each LULC grid required by the model (Sharp et al., 2020). The LULC_veg determines which AET calculation formula to be used. LULC with vegetation cover is assigned as 1, and others are assigned as 0. K_c is the evapotranspiration coefficient of vegetation, which is based on alfalfa, and used to adjust the ET_0 to obtain PET, with a range from 0.0 to 1.5. Root depth (Fig. 2b) is the maximum depth that plant

root system can extend, which is often expressed as the depth at which 95% of root biomass occurs (Allen et al., 2006). The data in Table 2 were obtained from the relevant literature (Yang et al., 2020), and from the values recommended by the FAO and the InVEST model.

Table 2 Biophysical table for the InVEST model

Code	Land use type	LULC_veg	K_c	Root depth (m)
1	Farmland	1	0.65	400
2	Forestland	1	1.00	1500
3	Grassland	1	0.65	500
4	Water body	0	1.00	1
5	Construction land	0	0.30	1
6	Unused land	0	0.50	1

Note: LULC_veg, land use/land cover with vegetation cover; K_c, evapotranspiration coefficient.

2.3.3 Model calibration

The InVEST model simulates natural runoff of a basin. The simulation accuracy largely depends on parameter Z (Eq. 3). The present study validated the parameter Z by comparing the simulated water yield data with natural runoff data at the Huaxian and Zhuangtou hydrological stations in the WRB from 1980 to 1984. The accuracy of simulation was assessed using the correlation coefficient (R^2), Nash coefficient (NSE), and relative error (R_e) (Rientjes et al., 2011). The study set the range of Z value for the study area to 3.6–9.0, consistent with those of relevant studies (Wu et al., 2018; Yue et al., 2021). The model was initiated with a Z value of 3.6, following which Z was gradually increased by 0.2. The process was continued until the maximized values of R^2, NSE, and R_e were obtained. After nearly a thousand tests, the optimal values of R_e, R^2, and NSE of 2%, 0.98, and 0.63, respectively were obtained at an input Z value of 8.8.

2.4 Trend analysis

Mann-Kendall (M-K) test is a non-parametric method, which does not need samples to follow a certain distribution, and is not disturbed by a few outliers (Mann, 1945; Kendall, 1975). The M-K test is often used to identify trends in precipitation and drought under the influence of climate change (Sheng and Paul, 2004). This study applied M-K test to detect the trends in the water yield, and climate factors over time. It should be noted that the statistic Z value from the M-K test is different to the seasonal parameter Z required as input into the InVEST model.

2.5 Correlation analysis

2.5.1 Global spatial autocorrelation

The present study used Moran's I to express global spatial autocorrelation. This index was used to analyze the overall correlations between spatial units, and to assess whether a spatial agglomeration existed. The valueof Moran's I ranges from −1 to 1. I>0 indicates that spatial attribute value has a spatial agglomeration effect with the surrounding attribute value, and the closer to 1 the I value, the more significant the spatial agglomeration effect. I<0 indicates that the spatial attribute value has a spatial difference effect with the surrounding attribute value. The spatial difference expressed by Moran's I becomes more significant, and the closer the value is to −1, whereas I=0 indicates no spatial autocorrelation (Tu and Xia, 2008). The spatial weight matrix was set as a simple binary adjacency matrix. The calculation of Moran's I is as follows (Moran, 1950):

$$I = \frac{n}{\sum i \sum j W_{ij}} \frac{\sum i \sum j W_{ij} \left(x_i - \overline{x}\right)\left(x_j - \overline{x}\right)}{\sum i \left(x_i - \overline{x}\right)^2}, \tag{7}$$

where W_{ij} is the spatial weight matrix of cell i and j; x_i and x_j are the measured values of cell x and y, respectively; $\overline{x}$ is the average measured value of all cells; and n is the number of all

evaluation units.

2.5.2 Bivariate local Moran's *I*

We used local indicators of spatial association (LISA) method to assess the strength of the correlation between attributes of each spatial unit and the attributes of adjacent units according to local Moran's *I* (Harries, 2006). Here, $I_i>0$ indicates that spatial units are highly correlated, including high-high and low-low types; $I_i<0$ indicates large differences in spatial units, including high-low and low-high types. The formula is as follows (Tepanosyan et al., 2019):

$$I_i = \frac{n^2}{\sum i \sum jW_{ij}} \frac{(x_i - \overline{x}) \sum jW_{ij}(x_j - \overline{x})}{\sum j(x_j - \overline{x})^2}. \quad (8)$$

This method can be used to study the spatial agglomeration effect of meteorological factors and water yield. The high-high and low-low types refer to proportional relationships between meteorological factors and water yield, whereas high-low and low-high types indicate inverse correlations.

3 Results

3.1 Spatiotemporal characteristics of water yield

3.1.1 Temporal variation

P, AET, PET, and simulated water yield in the WRB from 1985 to 2019 were shown in Figure 3. Annual average *P* over the study period was 542.09 mm with no significant temporal trend (Z=1.28, P>0.05). The minimum and maximum *P* of 364.26 and 766.12 mm occurred in 1997 and 2003, respectively. The average PET was 695.55 mm, showing no significant trend (Z=0.43, P>0.05). The average AET was 458.81 mm, and showed a significant increasing trend (Z=1.93, P<0.05), suggesting that more than 80.00% of precipitation in the WRB was returned to the atmosphere in the form of evaporation every year. The water yield of the WRB fluctuated, and was correlated with precipitation. The maximum and minimum water yields of 261.62 and 6.08

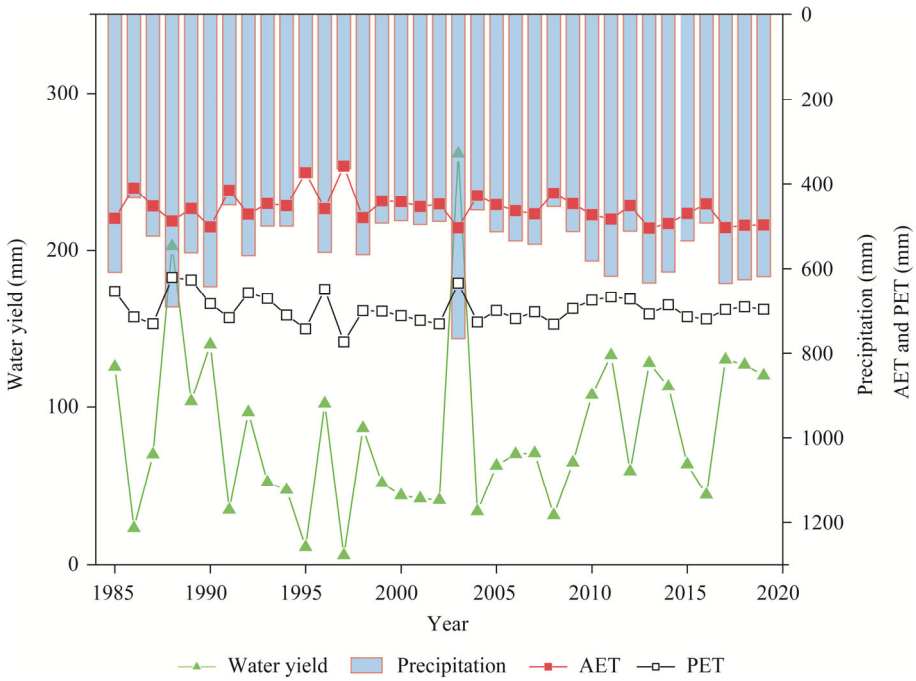

Fig. 3 Annual precipitation, actual evapotranspiration (AET), potential evapotranspiration (PET) and water yield of the Weihe River Basin, China during 1985−2019

mm were found in 2003 and 1997, respectively. The annual average water yield was 83.14 mm, accounting for about 15.33% of annual precipitation. There was an insignificantly increasing trend in water yield over the entire study period (Z=0.94, P>0.05) at a rate of 4.84 mm/10 a, with a turning point occurring in 2003.

3.1.2 Spatial variation

As shown in Figure 4, the present study examined the spatial distributions of simulated annual water yield. For example, in 1985, the overall water yield of the basin was high. The main water producing areas were located in the Beiluo River Basin, the north Jinghe River Basin, and the upper reaches of the Weihe River. The annual water yield from 2005 to 2015 decreased from east to west and south to north. The main water-producing areas included the main stream of the Weihe River, and southern part of the Qinling Mountains. The low water yield areas located in the Jinghe River and Beiluo River. The global Moran's I obtained by the Geoda model ranged from 0.38 to 0.68, indicating that water yield had a significant spatial agglomeration effect.

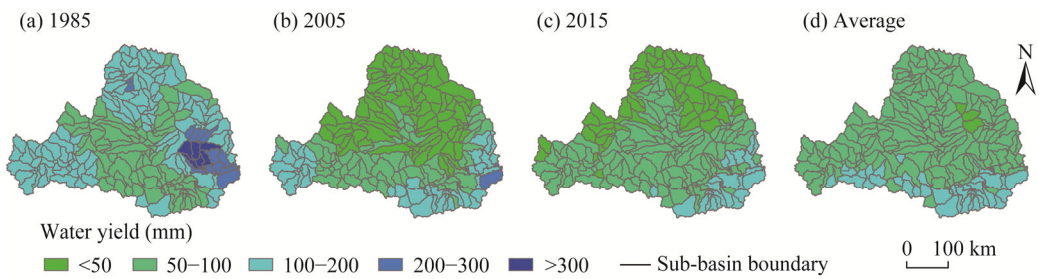

Fig. 4 Spatial distribution of water yield in the Weihe River Basin, China. (a), 1985; (b), 2005; (c), 2015; (d), average.

3.2 Response of water yield to *P* and LULC

According to the principle of water yield model, P and AET were the main factors affecting the simulation results. However, AET was largely influenced by LULC. In this study, two scenarios were designed to explore the changes in water yield under different LULC and P conditions (Table 3). Scenario 1 was established to study the change in water yield under different P intensities, in which 1997, 2003, and 2010 represented dry, wet, and average years, respectively. Scenario 2 was established to study the change in water yield under different LULC conditions.

Table 3 P and LULC under different scenarios

Index	Scenario 1			Scenario 2		
P	1997	2003	2007	1990	1990	1990
LULC	2020	2020	2020	1990	2010	2020

Note: P, precipitation; LULC, land use/land cover.

3.2.1 Change in water yield under scenario 1

The results of scenario 1 showed that water yield of the basin has changed significantly under different P conditions (Fig. 5). As P changed from less to more, the water yield of the basin changed accordingly. The maximum water yield during a wet year (675.40 mm) exceeded that during a dry year (133.53 mm) by a factor of 5, whereas it exceeded that during a normal year (365.20 mm) by a factor of 2. The average water yield of the basin varied greatly with changing P in 1997, 2003, and 2010 with 6.36, 264.63, and 72.96 mm, respectively. The spatial distribution of water yield was consistent with that of P. P in the study area was mostly concentrated in the southern and eastern areas, corresponding with the main water-producing areas of the WRB.

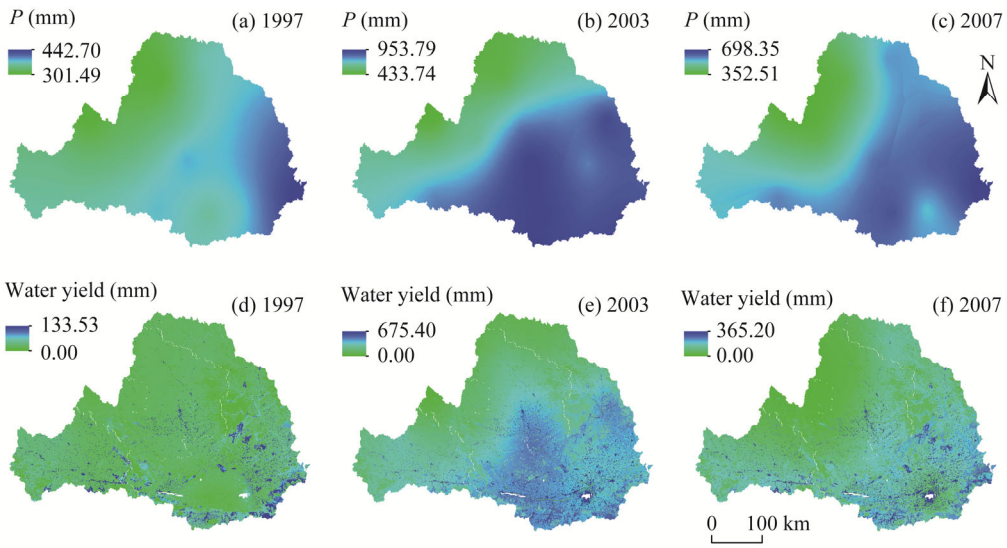

Fig. 5 Spatial distributions of annual precipitation (*P*, a–c) and water yield (d–f) in the Weihe River Basin, China under scenario 1

3.2.2 Spatial correlation between water yield and *P*

The bivariate Moran's *I* of *P* and water yield obtained by the Geoda model ranged from 0.30 to 0.80, and showed a positive correlation ($P>0.05$). The LISA agglomeration maps of *P* and water yield showed aggregations of mainly high-high and low-low correlation relationships (Fig. 6). Areas with high-high relationships were mainly concentrated in the southern and eastern WRB. Areas with low-low relationships were mainly concentrated in northern Jinghe River and Beiluo River.

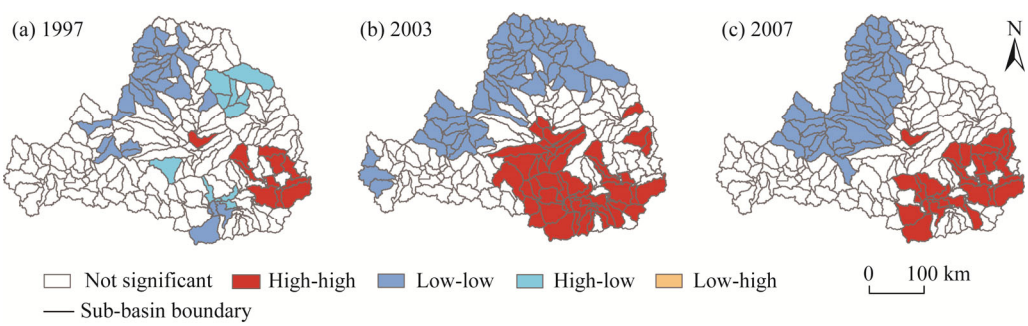

Fig. 6 Spatial distribution of the relationship between annual precipitation and water yield in the Weihe River Basin, China in 1997 (a), 2003 (b) and 2007 (c)

3.2.3 Change in water yield under scenario 2

The results of scenario 2 showed that LULC had no significant effect on water yield, but had an impact on the spatial distribution of water yield (Fig. 7). There were little differences between the maximum and average water yield of the basin in 1990, 2010, and 2019 with 468.10, 466.88, and 474.54 mm, respectively, and with 140.07, 140.9, and 142.85 mm, respectively. The distribution of land use types has a certain impact on the spatial characteristics of water yield. As shown in Figure 7, areas of higher water yield were correlated with grassland and farmland, such as northern Jinghe River and the upper reaches of the Weihe River.

3.2.4 Water yield under different LULC

The spatial analysis of ArcGIS10.2 was used to identify zones of water yield for each land use type under scenario 2. As shown in Figure 8, the fluctuations of water yield were different among

different LULC. The water yields of farmland, forestland, grassland, water body, and construction land continued to increase over the study period, whereas those of unused land first increased and then decreased. The maximum and minimum average water yield obtained for unused land and water body were 162.40 and 131.58 mm, respectively.

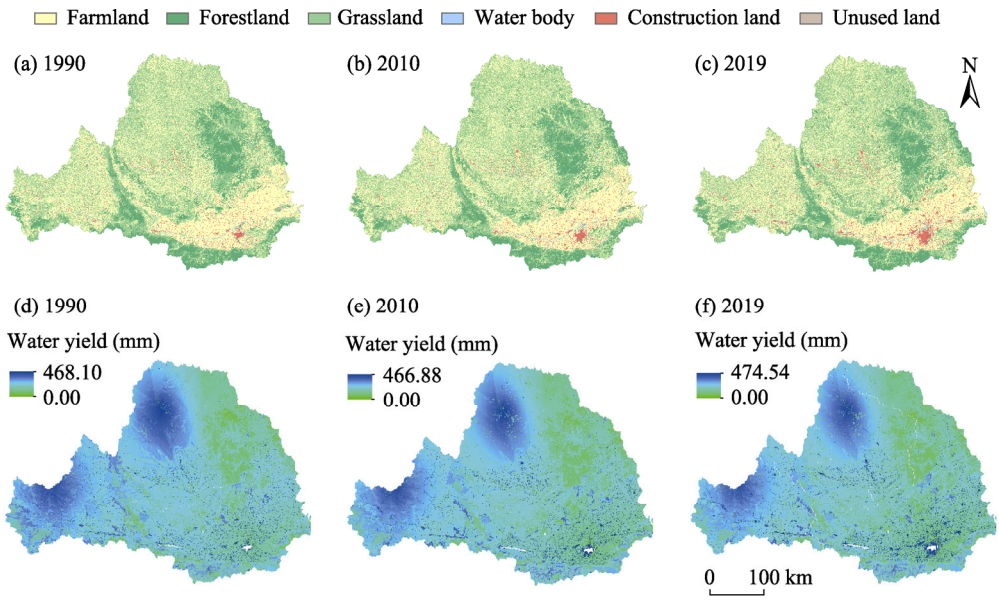

Fig. 7 Spatial distributions of LULC (land use/land cover) types (a–c) and water yield (d–f) in the Weihe River Basin, China under scenario 2

LULC of the WRB has changed significantly during the study period. As shown in Table 4, the areas of farmland, grassland, and construction land have changed significantly. Farmland area decreased by 4146.83 km^2, whereas water yield increased by 20.00 mm. The areas of forestland, grassland and construction land increased by 498.42, 1624.8, and 1791.96 km^2, respectively, whereas water yield increased by 11.34, 24.31, and 12.53 mm, respectively. The area of unused land decreased by 9.71 km^2, whereas water yield decreased by 17.44 mm. The results indicated that the areas of forestland, grassland, unused land, and water body had positive correlations with water yield, whereas that of farmland had a negative correlation with water yield. However, grassland and farmland were the dominant land use types in the WRB, accounting for more than 80% of the basin's area in 2020. Therefore, water yield was larger in grassland and agricultural land.

Table 4 Changes of LULC (land use/land cover) types of the Weihe River Basin China from 1990 to 2020

Index	Farmland (km^2)	Forestland (km^2)	Grassland (km^2)	Construction land (km^2)	Unused land (km^2)	Water body (km^2)	Total (km^2)
Farmland	32,855.50	3589.30	18,335.17	3383.78	68.70	491.49	58,723.94
Forestland	2933.04	11,916.83	6314.91	177.19	30.31	60.66	21,432.95
Grassland	16,536.86	6219.80	25,866.74	703.06	58.78	207.40	49,592.64
Construction land	1770.24	117.94	448.83	741.28	4.94	43.82	3127.04
Unused land	61.76	39.77	60.20	7.99	36.59	3.86	210.16
Water body	419.71	47.73	191.59	85.70	1.14	128.26	874.14
Total	54,577.11	21,931.37	51,217.44	5099.00	200.45	935.50	133,960.87

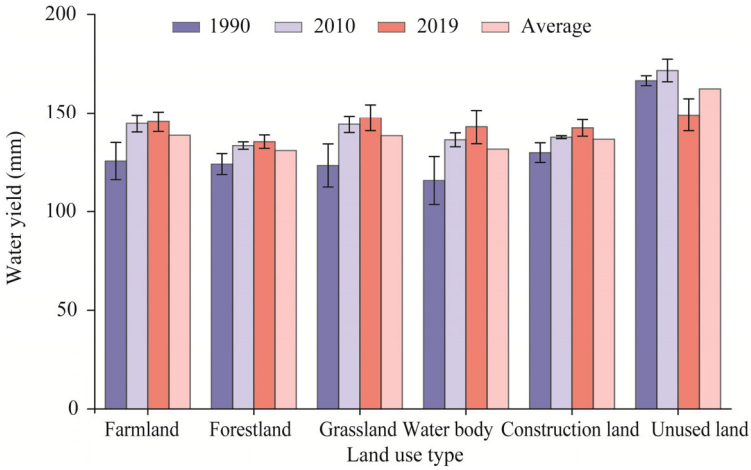

Fig. 8 Water yield of different LULC (land use/land cover) types in the Weihe River Basin, China

4 Discussion

4.1 Effects of various factors on water yield

A combined examination of the results of trend and spatial analysis as well as scenario analysis showed that precipitation was the most direct factor affecting regional water yield, which is consistent with the relevant research results (Jiang et al., 2016; Li et al., 2021). As for AET, it directly participates in the hydrological cycle process (Lewis and Allen, 2017). With emergence of challenges resulting from global climate change, AET has gradually increased in recent decades (Fig. 3). The increase in AET may accelerate the hydrological cycle process, and affect the temporal and spatial distributions of hydrological elements (Gusev et al., 2019; Cheng and Li, 2020). AET is not only affected by meteorological factors (temperature, wind speed, relative humidity and sunshine hours), but also by the land use conditions (Lang et al., 2017).

There is variation in water yield among different land use types due to differences in soil water content, evapotranspiration capacity, litter water holding capacity, and canopy interception. Unused land had the largest water yield because a greater proportion of precipitation directly penetrated into the ground or formed surface runoff (Lang et al., 2017). The increase in construction land in the basin has not only increased the demand for water resources, but also changed the underlying surface conditions. Construction practices transform the ground surface into an impermeable layer by removing the vegetation. These conditions lead to a decrease in the evapotranspiration and a higher water yield capacity (Sterling et al., 2013; Anache et al., 2017). The water yield capacity of water body is weak due to strong evaporation on the water surface. The water yield generated by forestland was relatively lower because of high transpiration and interception of water by the deep root system, litter layer, and dense canopy (Vose et al., 2011; Li et al., 2021). The effect of grassland and farmland on the redistribution of precipitation was similar to that of forestland. However, the regulation effect of grassland and farmland was relatively weak due to a lower canopy coverage and shallower root depth. In addition, the wide distributions of these two types of lands in the basin has resulted in their dominant contributions to water yield. Previous studies have shown that grassland was the optimal land use patterns for maintaining hydrology (Li et al., 2021). Although there have been considerable changes to the land use in the basin during the study period, these changes had no significant effect on water yield. This result can be attributed to the mutual transformation of various land types offsetting any dominant trend in water yield change due to land use changes (Nie et al., 2011).

Land use is the product of human activities, emphasizing human use of natural lands (Lambin et al., 2003; Goldewijk and Ramankutty, 2004; Liu et al., 2013), which can affect processes and

components of ecosystems. A series of soil and water conservation projects have been conducted in the basin since the 1950s (Mu et al., 2007). These include the construction of terraces and sediment dams, afforestation, plant restoration, pasture improvement, and the returning of farmland to forestland or grassland. These projects have significantly improved the ecological environment and water supply functions of the basin (Wang et al., 2017; He et al., 2021). The principle of water balance indicates that the difference between water yield and measured runoff is the water consumed by agricultural, urban and industrial activities, and the changes in reservoir storage (Li et al., 2020). The current study calculated the runoff of the WRB as sum of measured runoff of the Huaxian and Zhuangtou hydrological stations (Fig. 1) over years. The results showed an upward trend in annual water consumed (Z=1.56, P<0.01), which has increased pressure on water resources.

4.2 Limitations of the InVEST model

The InVEST model has been broadly used to evaluate ecosystem service functions, and has achieved good results (Lang et al., 2017; Kim and Jung, 2020; Daneshi et al., 2021). However, there are some uncertainties in the model related to model setup and its simplified algorithm (Sharp et al., 2020). For example, the model does not consider complex terrain factors, and is not able to rigorously describe the water balance process under complex underlying surface conditions (Jiang et al., 2016). Topography affects the climate by changing regional hydrothermal conditions. These changes influence the growth and structure of vegetation, the accumulation of litter and the physicochemical properties of soil, which consequently affect water yield (Jia et al., 2014; Maurya et al., 2016).

In addition, the present study obtained root depth and soil data for input into the model from the global soil database. The low spatial resolution of these data affected the simulation accuracy of the model to a certain extent. Moreover, the value of seasonal parameter Z used in the present study was slightly different from that applied in similar watersheds. This indicates that differences in natural conditions will lead to large changes in Z, even between similar basins. Therefore, the value of Z is important to verify before the InVEST model is applied.

5 Conclusions

The Weihe River is the largest tributary of the Yellow River, and has strategic significance for the protection of ecological environment and water resources management in Northwest China. The present study applied the InVEST model to quantitatively evaluate the water yield of the WRB from 1985 to 2019. In addition, the response of water yield to climate factors and land use types was explored.

The average annual water yield of the study area was 83.14 mm, and yearly water yield over the study period showed a slight increasing trend. The main stem of the Weihe River and southern region were the main water-producing areas. Water yield was comprehensively affected by climate and land use factors. Precipitation was the most direct influencing factor, with the spatial distribution of precipitation corresponding with that of water yield. In contrast, land use did not have a significant effect on water yield. However, there was variation in water yield among different land use types. Unused land had the largest water yield capacity, but farmland and grassland contributed the most to the total water yield of the basin due to their wide distribution. The results of the present study can act as a reference for formulating reasonable and efficient water resources allocation schemes. In addition, the successful application of the InVEST model in the current study can guide its application in related researches under similar natural conditions.

Acknowledgements

This work was funded by the National Natural Science Foundation of China (U2243211).

References

Allen R G, Prtrits L D, Raes D, et al. 2006. Crop evapotranspiration-guidelines for computing crop water requirements. Fao Irrigation & Drainage Paper No. 56. FAO, Rome, Italy.

Anache J A A, Flanagan D C, Srivastava A, et al. 2017. Land use and climate change impacts on runoff and soil erosion at the hillslope scale in the Brazilian Cerrado. Science of the Total Environment, 622–623: 140–151.

Baker T J, Miller S N. 2013. Using the soil and water assessment tool (SWAT) to assess land use impact on water resources in an East African watershed. Journal of Hydrology, 486: 100–111.

Boumans R, Costanza R. 2008. The multiscale integrated Earth systems model (MIMES): The dynamics, modeling and valuation of ecosystem services. Issues in Global Water System Research, 2(2): 30–41.

Budyko M I. 1974. Climate and Life. Academic Press: San Diego, 508

Cara A, Slhb A, Capm B. 2020. Modeling interactions among multiple ecosystem services. A critical review. Ecological Modelling, 429: 109103, doi: 10.1016/j.ecolmodel.2020.109103.

Chen Z S, Chen Y N, Li B F. 2013. Quantifying the effects of climate variability and human activities on runoff for Kaidu River Basin in arid region of northwest China. Theoretical and Applied Climatology, 111(3–4): 537–545.

Cheng B, Li H E, Yue S Y, et al. 2019. A conceptual decision-making for the ecological base flow of rivers considering the economic value of ecosystem services of rivers in water shortage area of Northwest China. Journal of Hydrology, 578: 124126, doi: 10.1016/j.jhydrol.2019.124126.

Cheng B, Li H. 2020. Impact of climate change and human activities on economic values produced by ecosystem service functions of rivers in water shortage area of Northwest China. Environmental Science and Pollution Research, 27(21): 26570–26578.

Costanza R, Arge R, Groot R, et al. 1998. The value of the world's ecosystem services and natural capital. Ecological Economics, 25(1): 3–15.

Daneshi A, Brouwer R, Najafinejad A, et al. 2021. Modelling the impacts of climate and land use change on water security in a semi-arid forested watershed using InVEST. Journal of Hydrology, 593: 125621, doi: 10.1016/j.jhydrol.2020.125621.

Dennedy-Frank P J, Muenich R L, Chaubey I, et al. 2016. Comparing two tools for ecosystem service assessments regarding water resources decisions. Journal of Environmental Management, 177: 331–340.

Donohue R J, Roderick M L, McVicar T R. 2012. Roots, storms and soil pores: Incorporating key ecohydrological processes into Budyko's hydrological model. Journal of Hydrology, 436–437: 35–50.

Droogers P, Allen R G. 2002. Estimating reference evapotranspiration under inaccurate data conditions. Irrigation and Drainage Systems, 16(1): 33–45.

Ercin A E, Hoekstra A Y. 2014. Water footprint scenarios for 2050: A global analysis. Environment International, 65(1): 71–82.

Fu B P. 1981. On the calculation of the evaporation from land surface. Scientia Atmospherica Sinica, 5(1): 23–31. (in Chinese)

Gassman P W, Reyes M R, Green C H, et al. 2007. The soil and water assessment tool: Historical development, applications, and future research directions. Transactions of the Asabe, 50(4): 1211–1250.

Goldewijk K K, Ramankutty N. 2004. Land cover change over the last three centuries due to human activities: The availability of new global data sets. Geojournal, 61(4): 335–344.

Gómez C M, Pérez-Blanco C D, Batalla R J. 2014. Tradeoffs in river restoration: Flushing flows vs. hydropower generation in the Lower Ebro River, Spain. Journal of Hydrology, 518: 130–139.

Gusev E M, Nasonova O N, Kovalev E E, et al. 2019. Impact of possible climate change on extreme annual runoff from river basins located in different regions of the globe. Water Resources, 46: S126–S136.

Harries K. 2006. Extreme spatial variations in crime density in Baltimore County, MD. Geoforum, 37(3): 404–416.

Hassan R, Scholes R, Ash N. 2005. Ecosystems and human well-being: Current state and trends. Journal of Bacteriology, 1(5): 1387–1404.

He J, Shi X Y, Fu Y J. 2021. Identifying vegetation restoration effectiveness and driving factors on different micro-topographic types of hilly Loess Plateau: From the perspective of ecological resilience. Journal of Environmental Management, 289: 112562, doi: 10.1016/j.jenvman.2021.112562.

Huang C H, Yang J, Zhang W J. 2013. Development of ecosystem services evaluation models: Research progress. Chinese Journal of Ecology, 32(12): 3360–3367. (in Chinese)

Jia X, Fu B, Feng X, et al. 2014. The tradeoff and synergy between ecosystem services in the Grain-for-Green areas in northern Shaanxi, China. Ecological Indicators, 43(1): 103–113.

Jiang C, Li D Q, Wang D W, et al. 2016. Quantification and assessment of changes in ecosystem service in the Three-River Headwaters Region, China as a result of climate variability and land cover change. Ecological Indicators, 66: 199–211.

Jiang H Q, Wu W J, Wang J N, et al. 2021. Mapping global value of terrestrial ecosystem services by countries. Ecosystem Services, 52: 101361, doi: 10.1016/j.ecoser.2021.101361.

Kendall M G. 1975. Rank correlation methods. Charles Griffin: London. British Journal of Psychology, 25(1): 86–91.

Kim S W, Jung Y Y. 2020. Application of the InVEST model to quantify the water yield of North Korean forests. Forests, 11(8): 804.

Lambin E F, Geist H J, Lepers E. 2003. Dynamics of land-use and land-cover change in tropical regions. Annual Review of Environment and Resources, 28(1): 205–241.

Lang Y, Song W, Zhang Y. 2017. Responses of the water-yield ecosystem service to climate and land use change in Sancha River Basin, China. Physics and Chemistry of the Earth, Parts A/B/C: 102–111.

Lewis C S, Allen L N. 2017. Potential crop evapotranspiration and surface evaporation estimates via a gridded weather forcing dataset. Journal of Hydrology, 546: 450–463.

Li M Y, Liang D, Xia J, et al. 2021. Evaluation of water conservation function of Danjiang River Basin in Qinling Mountains, China based on InVEST model. Journal of Environmental Management, 286: 112212, doi: 10.1016/j.jenvman.2021.112212.

Li X Y, Guo J M, Qi S Z. 2021. Forestland landscape change induced spatiotemporal dynamics of subtropical urban forest ecosystem services value in forested region of China: A case of Hangzhou City. Environmental Research, 193: 110618, doi: 10.1016/j.envres.2021.110926.

Li Y Y, Yao S B, Deng Y J, et al. 2020. Spatio-temporal study on supply and demand matching of ecosystem water yield service–a case study of Wei River Basin. Polish Journal of Environmental Studies, 30(2): 1677–1693.

Liu J, Wu Y. 2012. Water sustainability for China and beyond. Science, 337(6095): 649–650.

Liu J X, Li Z G, Zhang X P, et al. 2013. Responses of vegetation cover to the Grain for Green program and their driving forces in the He-Long region of the middle reaches of the Yellow River. Journal of Arid Land, 5(4): 511–520.

Liu Y, Hu A M. 2008. Study on spatial differentiation characteristics of water resources supply-demand and balance in Weihe Basin. Journal of Arid Land Resources and Environment, 22(3): 81–85.

Ma Z M, Kang S Z, Zhang L, et al. 2008. Analysis of impacts of climate variability and human activity on streamflow for a river basin in arid region of northwest China. Journal of Hydrology, 352(3–4): 239–249.

Mann H B. 1945. Nonparametric test against trend. Econometrica, 13(3): 245–259.

Maurya S, Srivastava P K, Gupta M, et al. 2016. Integrating soil hydraulic parameter and micro wave precipitation with morphometric analysis for watershed prioritization. Water Resources Management, 30(14): 5385–5405.

Mekonnen M M, Hoekstra A Y. 2016. Four billion people facing severe water scarcity. Science Advances, 2(2): e1500323, doi: 10.1126/sciadv.1500323.

Milliman J D, Farnsworth K L, Jones P D, et al. 2008. Climatic and anthropogenic factors affecting river discharge to the global ocean, 1951–2000. Global and Planetary Change, 62(3–4): 187–194.

Moran P A P. 1950. Notes on continuous stochastic phenomena. Biometrika, 37(1–2): 17–23.

Mu X M, Zhang L, McVicar T R, et al. 2007. Analysis of the impact of conservation measures on stream flow regime in catchments of the Loess Plateau, China. Hydrological Processes, 21(16): 2124–2134.

Natalia P, Silvia F, Laura B, et al. 2015. Getting water right: A case study in water yield modelling based on precipitation data. Science of the Total Environment, 537: 225–234.

Nie W, Yuan Y, Kepner W, et al. 2011. Assessing impacts of land use and land cover changes on hydrology for the upper San Pedro watershed. Journal of Hydrology, 407(1–4): 105–114.

Qiang Z, Xu C Y, Tao Y. 2009. Scaling properties of the runoff variations in the arid and semi-arid regions of China: A case study of the Yellow River basin. Stochastic Environmental Research & Risk Assessment, 23(8): 1103–1111.

Qiu J. 2010. China faces up to groundwater crisis. Nature, 466(7304): 308–308.

Rientjes T, Perera B, Haile A T, et al. 2011. Regionalisation for lake level simulation–the case of Lake Tana in the upper Blue Nile, Ethiopia. Hydrology and Earth System Sciences Discussions, 15(14): 1167–1183.

Scordo F, Lavender T M, Seitz C, et al. 2018. Modeling water yield: Assessing the role of site and region-specific attributes in determining model performance of the InVEST seasonal water yield model. Water, 10(11): 1496, doi: 10.3390/w10111496.

Sharp R, Douglass J, Wolny S, et al. 2020. InVEST 3.9.0 User's Guide. The Natural Capital Project, Stanford University, University of Minnesota, the Nature Conservancy and World Wildlife Fund.

Sheng Y, Paul P. 2004. A comparison of the power of the *t* test, Mann-Kendall and bootstrap tests for trend detection: Detecting change in hydrological data. International Association of Scientific Hydrology Bulletin, 49(1): 21–37.

Sherrouse B C, Clement J M, Semmens D J. 2011. A GIS application for assessing, mapping, and quantifying the social values of ecosystem services. Applied Geography, 31(2): 748–760.

Sterling S M, Ducharne A, Polcher J. 2013. The impact of global land-cover change on the terrestrial water cycle. Nature

Climate Change, 3(4): 385–390.

Symmank L, Natho S, Scholz M, et al. 2020. The impact of bioengineering techniques for riverbank protection on ecosystem services of riparian zones. Ecological Engineering, 158: 106040, doi: 10.1016/j.ecoleng.2020.106040.

Tepanosyan G, Sahakyan L, Zhang C S, et al. 2019. The application of local Moran's *I* to identify spatial clusters and hot spots of Pb, Mo and Ti in urban soils of Yerevan. Applied Geochemistry, 104: 116–123.

Tu J, Xia Z G. 2008. Examining spatially varying relationships between land use and water quality using geographically weighted regression *I*: Model design and evaluation. Science of the Total Environment, 407(1): 358–378.

Vorosmarty C J, Green P, Salisbury J, et al. 2000. Global water resources: Vulnerability from climate change and population growth. Science, 289(5477): 284–288.

Vose J M, Sun G, Ford C R, et al. 2011. Forest ecohydrological research in the 21st century: What are the critical needs? Ecohydrology, 4(2): 146–158.

Wang B, Gao P, Niu X, et al. 2017. Policy-driven China's Grain to Green program: Implications for ecosystem services. Ecosystem Services, 27: 38–47.

Wu N, Song X Y, Kang W H, et al. 2018. Standard of payment for ecosystem services in a watershed based on InVEST model under different standpoints: A case study of the Weihe River in Gansu Province. Acta Ecologica Sinica, 38(7): 2512–2522. (in Chinese)

Xia J, Qiao Y F, Song X F, et al. 2007. Analysis about effect rules of underlying surface change to the relationship between rainfall and runoff in the Chabagou Catchment. Resources Science, 29(1): 70–76. (in Chinese)

Xu K, Milliman J D, Hui X. 2010. Temporal trend of precipitation and runoff in major Chinese rivers since 1951. Global and Planetary Change, 73(3–4): 219–232.

Xu Y X, Zhu G F, Wan Q Z, et al. 2021. Effect of terrace construction on soil moisture in rain-fed farming area of Loess Plateau. Journal of Hydrology: Regional Studies, 37: 100889, doi: 10.1016/j.ejrh.2021.100889.

Yang D, Liu W, Tang L, et al. 2019. Estimation of water provision service for monsoon catchments of South China: Applicability of the InVEST model. Landscape and Urban Planning, 182: 133–143.

Yang H B, Yang D W, Lei Z D, et al. 2008. New analytical derivation of the mean annual water-energy balance equation. Water Resources Research, 44(3): 893–897.

Yang J, Xie B P, Zhang D G. 2020. Spatio-temporal variation of water yield and its response to precipitation and land use change in the Yellow River Basin based on InVEST model. Chinese Journal of Applied Ecology, 31(8): 2731–2739. (in Chinese)

Yang X, Chen R S, Meadows M E, et al. 2020. Modelling water yield with the InVEST model in a data scarce region of northwest China. Water Supply, 20(3): 1035–1045.

Yin G D, Wang X, Zhang X, et al. 2020. InVEST model-based estimation of water yield in North China and its sensitivities to climate variables. Water, 12(6): 1692, doi: 10.3390/w12061692.

Yue S Y, Li H E, Zhao L. 2021. Impact of climate and land use changes on water scarcity in the Wei River Basin. Research of Soil and Water Conservation, 28(5): 95–101. (in Chinese)

Zhang H, Huang Q, Zhang Q, et al. 2016. Changes in the long-term hydrological regimes and the impacts of human activities in the main Wei River, China. Hydrological Sciences Journal, 61(6): 1054–1068.

Zhang L, Hickel K, Dawes W R, et al. 2004. A rational function approach for estimating mean annual evapotranspiration. Water Resources Research, 40(2): W02502, doi: 10.1029/2003WR002710.

Zhao Y, Hu C H, Zhang X M, et al. 2018. Analysis on runoff and sediment regimes and its causes of the Yellow River in recent 70 years. Transactions of the Chinese Society of Agricultural Engineering, 34(21): 112–119. (in Chinese)

Zhou W, Liu G, Pan J, et al. 2005. Distribution of available soil water capacity in China. Journal of Geographical Sciences, 15(1): 3–12.